Research Square

Preprints are preliminary reports that have not undergone peer review.
They should not be considered conclusive, used to inform clinical practice,
or referenced by the media as validated information.

Reliable X-Ray diffraction linewidth analysis of metastable cubic GaN thin films using baseline-corrected nonlinear peak fitting

Yoanlys Hernández Barrios
Centro de Investigación y de Estudios Avanzados del Instituto Politécnico Nacional
José A. Santis Espinosa
alfredo_santis@cinvestav.mx

Centro de Investigación y de Estudios Avanzados del Instituto Politécnico Nacional
Bellanirys Moreno Juan
Universidad Autónoma de Chiapas
José G. Sánchez López
Centro de Investigación y de Estudios Avanzados del Instituto Politécnico Nacional
Salvador I. Garduño Vértiz
Centro de Investigación y de Estudios Avanzados del Instituto Politécnico Nacional
José Juan DÍaz
Federico Santa María Technical University

Research Article

Keywords: cubic GaN, X-ray diffraction, pseudo-Voigt fitting, linewidth analysis, crystallite size, defect density

Posted Date: November 3rd, 2026

DOI: https://doi.org/10.21203/rs.3.rs-11272303/v1

License: This work is licensed under a Creative Commons Attribution 4.0 International License.
Read Full License

Additional Declarations: No competing interests reported.

Reliable X-Ray diffraction linewidth analysis of metastable cubic GaN thin films using baseline-corrected nonlinear peak fitting

Yoanlys Hernández Barrios[1], José A. Santis Espinosa[1,2*], Bellanirys Moreno Juan[3†], José G. Sánchez López[1†], Salvador I. Garduño Vértiz[1†], José Juan Díaz[1,4†]

[1]Department of Electrical Engineering, CINVESTAV, Av. Instituto Politécnico Nacional 2508 Mexico City, 07360, , Mexico.
[2*]Optic department, National Institute of Astrophysics, Optics and Electronics (INAOE), Luis Enrique Erro No. 1, Santa María Tonantzintla, 72840, Puebla, Mexico.
[3]Escuela de Ciencias Químicas, Universidad Autónoma de Chiapas (UNACH), Ocozocoautla de Espinosa, 29140, Chiapas, Mexico.
[4]Departamento de Física, Universidad Técnica Federico Santa María, Av. España 1680 Valparaíso , 2390123, Chile.

*Corresponding author(s). E-mail(s): alfredo_santis@cinvestav.mx;
Contributing authors: yoanlys.hernandez@cinvestav.mx; bellanirysjuan@gmail.com; jsanchezl@cinvestav.mx; sgarduno@cinvestav.mx; jose.diazl@usm.cl;
†These authors contributed equally to this work.

Abstract

Evaluating the crystalline quality of metastable cubic GaN (c-GaN) thin films requires reliable X-ray diffraction (XRD) linewidth analysis, which can be affected by defect-induced broadening and background contributions. This study systematically compares nonlinear fitting strategies for the c-GaN(200) reflection of films grown on GaP substrates by metal-organic chemical vapor deposition. Unconstrained pseudo-Voigt, fixed-mixing-parameter pseudo-Voigt, baseline-subtracted pseudo-Voigt, and baseline-corrected nonlinear Gaussian fitting were evaluated. Unconstrained pseudo-Voigt fitting artificially overestimated Lorentzian broadening due to background sensitivity, resulting in physically

inconsistent linewidths. In contrast, baseline-corrected nonlinear Gaussian fitting provided the most stable and physically consistent full width at half maximum evolution. Using this approach, a systematic linewidth reduction from S1 to S4 was observed, consistent with increased crystallite size and reduced defect density. These results demonstrate the importance of rigorous baseline correction and profile selection for reliable structural analysis of semiconductor thin films.

Keywords: cubic GaN; X-ray diffraction; pseudo-Voigt fitting; linewidth analysis; crystallite size; defect density.

1 Introduction

X-ray diffraction (XRD) peak-profile analysis is one of the most widely used methods for evaluating the structural quality of crystalline thin films. Beyond the identification of crystallographic phases, the position, shape, and width of diffraction peaks provide information related to lattice parameter variations, crystallite size, microstrain, mosaicity, and defect-related broadening [1, 2]. However, the quantitative extraction of these parameters is strongly dependent on the peak-shape function, baseline treatment, instrumental contribution, and fitting window used during the analysis. Therefore, selecting an appropriate fitting methodology is a critical step when comparing the crystalline quality of samples obtained under different growth conditions. This is particularly relevant for metastable polytypes such as cubic gallium nitride (c-GaN), which crystallizes in the zincblende structure and is typically stabilized through epitaxial growth on cubic substrates (e.g., GaAs or MgO) [3]. Due to its metastable nature and lattice mismatch with the substrate, c-GaN films often exhibit complex structural features, including wurtzite inclusions, high densities of stacking faults, and microtwins [4]. Consequently, a rigorous XRD peak-profile analysis becomes an essential tool not only for verifying phase purity and assessing lattice relaxation, but also for quantifying the microstructural defects inherent to the cubic polytype, where anisotropic peak broadening and specific peak asymmetries serve as direct signatures of stacking faults and twin boundaries.

Several analytical functions have been employed to describe XRD peak profiles, including Gaussian, Lorentzian, Voigt, and pseudo-Voigt functions. Gaussian profiles are commonly associated with instrumental broadening and statistical distributions of strain, whereas Lorentzian profiles are frequently related to size broadening and defect-induced tails. Because real diffraction peaks usually contain contributions from both Gaussian and Lorentzian broadening mechanisms, the pseudo-Voigt function, defined as a linear combination of both components, has become one of the most widely used approximations for XRD and neutron diffraction profile analysis. In particular, the Thompson–Cox–Hastings pseudo-Voigt formalism is commonly used in Rietveld refinement and line-profile analysis because it provides a practical description of peak broadening while reducing the computational cost associated with the full Voigt convolution [5–7].

Despite its widespread use, pseudo-Voigt fitting may lead to ambiguous or physically unstable results when the baseline, asymmetric tails, overlapping contributions, or low-intensity features are not properly constrained. In thin-film systems, these effects become particularly relevant because diffraction peaks may be broadened by a combination of finite crystallite size, residual strain, mosaic disorder, stacking faults, dislocations, and phase coexistence. As a result, unconstrained fitting procedures may yield excellent numerical fitting coefficients while still producing linewidths that are not physically meaningful. This limitation has motivated the use of comparative fitting strategies in which Gaussian, Lorentzian, pseudo-Voigt, and baseline-corrected models are evaluated in parallel to identify the most reliable approach for extracting full width at half maximum (FWHM), crystallite size, and defect-related parameters [8, 9].

The interpretation of XRD linewidths is also closely related to classical size-broadening models such as the Scherrer equation. Although the Scherrer method remains widely used for estimating coherent crystallite size from diffraction peak widths, its application requires careful consideration of instrumental broadening, peak-shape assumptions, and the physical meaning of the extracted FWHM values [10–12]. Moreover, broadening contributions from microstrain and defects may not be fully separable from size effects using a single-peak analysis. Consequently, linewidth-based structural parameters should be interpreted as effective indicators of crystalline coherence rather than absolute microstructural quantities unless supported by complementary analyses.

In cubic GaN heteroepitaxy, reliable linewidth analysis is particularly important because structural disorder, phase coexistence, and defect-induced broadening strongly affect the interpretation of crystalline quality evolution. Since the c-GaN(200) reflection is commonly used as a structural quality indicator, inaccuracies in peak fitting may lead to misleading estimations of crystallite size, strain, and defect density. Therefore, establishing a physically consistent fitting methodology is essential for the comparative evaluation of optimized growth routes in metastable cubic GaN systems [13–15].

In this work, different nonlinear fitting strategies were systematically evaluated for the c-GaN(200) XRD reflection of cubic GaN films grown on GaP substrates by metal-organic chemical vapor deposition. The fitting procedures included unconstrained pseudo-Voigt fitting, fixed-mixing-parameter pseudo-Voigt fitting, baseline-subtracted pseudo-Voigt fitting, and nonlinear Gaussian fitting. The objective was to determine how the selected peak-shape model and baseline correction affect the extracted FWHM, crystallite size, and estimated dislocation density. By comparing the results obtained from different fitting approaches, this study identifies the most physically consistent method for evaluating the evolution of crystalline quality in c-GaN films and demonstrates the importance of model selection in XRD peak-profile analysis of semiconductor thin films.

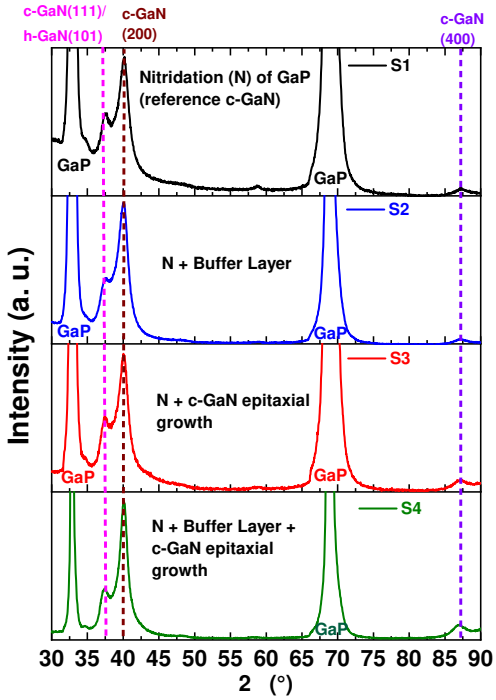


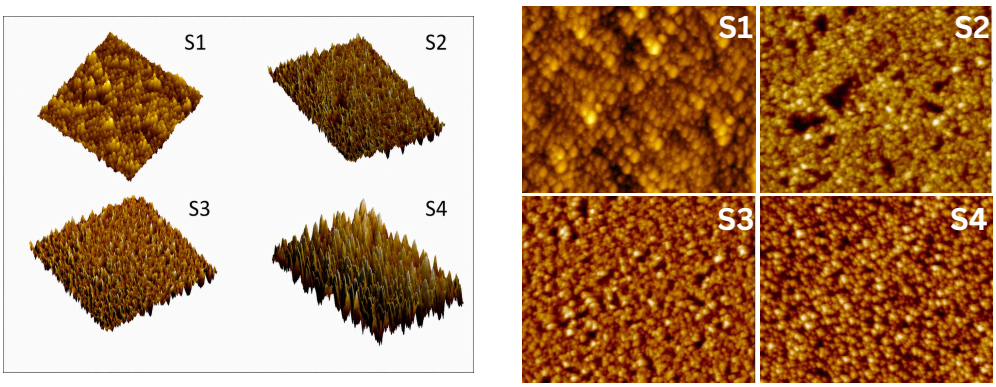
Fig. 1: XRD patterns of samples S1–S4 corresponding to the different stages of nitridation, buffer-layer deposition, and c-GaN epitaxial growth on GaP substrates. The characteristic c-GaN(111), c-GaN(200), and c-GaN(400) reflections are observed together with the GaP substrate peaks.

2 Sample Description and Characterization

2.1 Structural Characterization

The crystalline structure of the c-GaN layers grown on GaP substrates was investigated by X-ray diffraction (XRD). Figure 1 presents the diffraction patterns acquired from samples S1–S4, corresponding to the different stages of substrate nitridation, buffer-layer deposition, and c-GaN epitaxial growth.

In addition to the characteristic reflections of the GaP substrate, diffraction peaks associated with cubic GaN are observed near $2\theta \approx 37.5°$, 40°, and 86°, corresponding to the c-GaN(111) or the hexagonal GaN (101), c-GaN(200), and c-GaN(400) planes, respectively [16]. The presence of these reflections confirms the successful formation of the cubic GaN phase on the nitridated GaP surface. [13]. Significant variations in the intensity and full width at half maximum (FWHM) of the diffraction peaks were observed among the samples. These differences indicate changes in crystalline quality, crystallite size, and defect density, likely arising from the distinct growth sequences used during material synthesis [15].



(a) Direct growth. (b) Buffer-assisted growth.

Fig. 2: AFM topography images of (a) S1, (b) S2, (c) S3, and (d) S4. The images reveal the evolution of the surface morphology as a function of nitridation, buffer-layer growth, and c-GaN epitaxial growth.

Particular attention was devoted to the c-GaN(200) reflection because of its relatively high intensity and its isolation from neighboring substrate peaks. The progressive evolution of the peak shape and linewidth among the investigated samples suggests significant differences in the structural quality of the deposited layers. Therefore, the c-GaN(200) reflection was selected for the detailed peak-profile analysis presented in the following sections.

2.2 Surface Morphology Characterization

The surface morphology of the investigated samples was evaluated by atomic force microscopy (AFM). Representative AFM topography images are shown in Figure 2 for samples S1–S4.

Sample S1 exhibits an anisotropic surface texture, whereas samples incorporating the low-temperature GaN buffer layer show a more homogeneous granular morphology and improved surface organization. The nitridated reference sample (S1) is characterized by elongated surface features and directional grain growth. Following the introduction of the low-temperature GaN buffer layer (S2), the surface evolves toward a finer granular morphology with improved lateral uniformity, although isolated depressions remain visible. Sample S3, which underwent c-GaN epitaxial growth in the absence of a low-temperature buffer layer, exhibits a high density of nucleation centers and a granular surface morphology associated with the coalescence of crystalline islands [17, 18].

Among the investigated structures, sample S4, incorporating both nitridation and the low-temperature GaN buffer layer prior to c-GaN growth, presents the most homogeneous surface morphology. The surface is characterized by a compact grain distribution and a reduction in large-scale surface irregularities, suggesting improved lateral growth and enhanced surface organization [13].

The observed morphological evolution is consistent with the structural trends identified by XRD analysis. In particular, the improved surface uniformity observed for sample S4 correlates with the narrowing of the c-GaN(200) diffraction peak discussed in the following sections, indicating enhanced crystalline ordering and a reduced contribution of defect-related broadening mechanisms [19, 20].

3 Results and Discussion

3.1 Peak-Profile Analysis Methodology

Different fitting strategies were evaluated to determine the most appropriate approach for comparing the crystalline quality evolution of the films.

3.1.1 Unconstrained Pseudo-Voigt Fitting (U-PV)

As an initial approach, the c-GaN(200) diffraction peak was analyzed using an unconstrained pseudo-Voigt profile combined with a linear background contribution. In this methodology, the Gaussian and Lorentzian components were simultaneously optimized through a free mixing parameter (η), allowing the fitting routine to adapt to the experimental peak shape without additional physical constraints. The fitting procedure was performed over a broad angular range in order to include the complete diffraction profile and its surrounding background contribution. This initial analysis was employed to evaluate the general peak-shape behavior and to identify possible broadening effects associated with a slight asymmetry toward higher 2θ angles, background contributions, and defect-related linewidth distortions [21, 22].

The initial proposed approach employed a standard pseudo-Voigt profile combined with a linear background model as follows:

$$I(x) = I_{\mathrm{PV}}(x) + mx + b \tag{1}$$

where the pseudo-Voigt component is defined as:

$$I_{\mathrm{PV}}(x) = A\left[\eta L(x) + (1-\eta)G(x)\right] \tag{2}$$

with:

- A the peak amplitude,
- η the Lorentzian fraction,
- $L(x)$ the Lorentzian contribution,
- $G(x)$ the Gaussian contribution.

The Gaussian function is given by:

$$G(x) = \exp\left[-\frac{(x-x_0)^2}{2\sigma^2}\right] \tag{3}$$

with:

$$\sigma = \frac{\mathrm{FWHM}}{2\sqrt{2\ln 2}} \tag{4}$$

while the Lorentzian component is:

$$L(x) = \frac{\gamma^2}{(x - x_0)^2 + \gamma^2} \tag{5}$$

where:

$$\gamma = \frac{\text{FWHM}}{2} \tag{6}$$

3.1.2 Fixed-η Pseudo-Voigt Fitting (F-η-PV)

To reduce the excessive Lorentzian broadening observed in the unconstrained fitting procedure, a second analysis was performed using a pseudo-Voigt profile with a fixed mixing parameter [23]. In this approach, the Lorentzian-to-Gaussian contribution ratio was constrained by fixing $\eta = 0.5$, thereby preventing artificial profile distortions caused by unconstrained optimization of the peak shape. The selected η value corresponds approximately to the average obtained from the unconstrained fitting procedure. The value $\eta = 0.5$ was selected as a compromise between the Gaussian and Lorentzian contributions and was found to provide stable fitting results across all samples.

Additionally, the fitting window was reduced in order to minimize the influence of low-intensity background contributions and asymmetric peak tails. This recalibrated fitting strategy was implemented to obtain more physically consistent linewidth estimations suitable for comparative structural analysis among the different c-GaN samples. While the unconstrained fitting provides information on peak-shape evolution, the fixed-η approach facilitates a more reliable comparison of linewidth variations among samples.

3.1.3 Baseline-Corrected Pseudo-Voigt Fitting (BC-PV)

A further refinement of the linewidth analysis was implemented by introducing a local baseline subtraction procedure prior to the pseudo-Voigt fitting. In this methodology, the background contribution was estimated from the edges of the fitting window and subsequently removed from the experimental diffraction profile before peak fitting [23]. This approach minimizes artificial broadening associated with asymmetric background contributions and improves the physical consistency of the extracted linewidths. A linear baseline was determined from the average intensity values at both edges of the fitting interval. After baseline correction, the diffraction peak was fitted using a pseudo-Voigt profile with a predominantly Gaussian contribution obtained by fixing the mixing parameter to $\eta = 0.3$ while retaining a moderate Lorentzian contribution associated with structural defects such as dislocations, stacking faults, and local lattice distortions [24]. The η value provided the lowest fitting residuals while maintaining physically realistic linewidth values. The fitting range was further restricted to the central portion of the diffraction peak to minimize the influence of low-intensity tails and enhance the robustness of the linewidth determination.

In this approach, the background contribution was estimated from the edges of the fitting window and removed before fitting:

$$I_{\text{sub}}(x) = I(x) - I_{\text{baseline}}(x) \tag{7}$$

where the local linear baseline is:

$$I_{\text{baseline}}(x) = mx + b \tag{8}$$

This procedure minimizes:

- asymmetric tail contributions,
- baseline-induced broadening,
- background distortions.

3.1.4 Nonlinear Gaussian Fitting (BC-Gauss)

Based on the comparative analysis of the different fitting methodologies, a nonlinear Gaussian fitting procedure combined with local baseline subtraction was selected as the most stable approach for extracting comparative linewidth parameters. In this methodology, the experimental background was first estimated through a local linear baseline and subsequently removed from the diffraction profile. The corrected peak was then fitted using a Gaussian function in order to obtain reliable estimations of the full width at half maximum (FWHM) for comparative structural analysis. This method yielded the lowest fitting residuals and the smallest sample-to-sample linewidth uncertainty among the analyzed samples and minimized artificial broadening effects associated with background distortions and unconstrained Lorentzian contributions as discussed in the next section.

First, a linear baseline was estimated from the edges of the fitting window and subtracted from the experimental XRD intensity:

$$I_{\text{sub}}(2\theta) = I_{\text{exp}}(2\theta) - I_{\text{baseline}}(2\theta), \tag{9}$$

where the local baseline was described as

$$I_{\text{baseline}}(2\theta) = m(2\theta) + b. \tag{10}$$

The baseline-corrected diffraction peak was then fitted using a Gaussian function:

$$I_{\text{G}}(2\theta) = A \exp\left[-\frac{(2\theta - 2\theta_0)^2}{2\sigma^2}\right], \tag{11}$$

where A is the peak amplitude, $2\theta_0$ is the peak center, and σ is the standard deviation of the Gaussian profile. The full width at half maximum was obtained from:

$$\text{FWHM} = 2\sqrt{2\ln 2}\,\sigma. \tag{12}$$

3.2 Comparative Structural Linewidth Analysis

The different peak-profile fitting methodologies produced markedly different linewidth estimations for the c-GaN(200) diffraction reflection, highlighting the strong influence of profile-shape selection, fitting constraints, and baseline treatment on the extracted

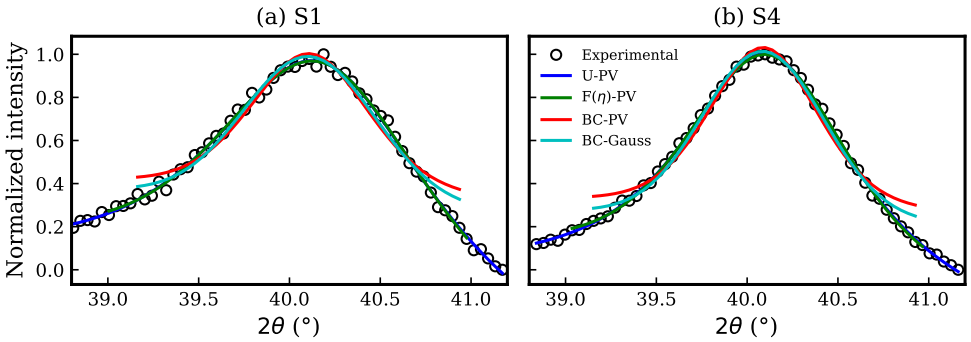


Fig. 3: Comparison between experimental XRD profiles and the fitted peak shapes obtained using the different fitting methodologies for samples S1 and S4. The figure illustrates the influence of profile-shape selection and baseline treatment on the representation of the c-GaN(200) diffraction peak.

structural parameters. Although all fitting approaches provided satisfactory numerical agreement with the experimental diffraction profiles, significant differences were observed in the resulting full width at half maximum (FWHM), crystallite size, and defect-density estimations [25].

Figure 3 compares the experimental diffraction profiles and the fitted curves obtained using the four analyzed methodologies for samples S1 and S4. The unconstrained pseudo-Voigt fitting exhibited an excellent agreement with the experimental data; however, the fitting procedure systematically converged toward a purely Lorentzian profile ($\eta \approx 1$). This behavior suggests a strong sensitivity of the fitting routine to asymmetric peak tails and residual background contributions, which can artificially broaden the extracted linewidth. The introduction of profile-shape constraints and baseline subtraction progressively reduced this effect, yielding more physically realistic peak shapes and linewidth estimations. The resulting linewidth values exhibited a monotonic decrease from S1 to S4. This trend is consistent with reduced structural disorder, lower defect-related broadening, and enhanced crystal coherence associated with the optimized growth conditions.

The evolution of the extracted FWHM values obtained from the different fitting methodologies is presented in Figure 4. The unconstrained pseudo-Voigt fitting yielded the largest FWHM values for all samples, ranging from approximately 1.57° for S1 to 1.21° for S4. This behavior is consistent with the predominance of the Lorentzian component observed during the fitting process, which tends to overemphasize peak tails and can lead to artificially enlarged linewidth estimations. Constraining the pseudo-Voigt mixing parameter to $\eta = 0.5$ reduced the extracted FWHM values; however, a slight non-monotonic variation between samples S1 and S2 remained apparent. The relationship between the extracted linewidths and the goodness-of-fit coefficients is further illustrated in Figure 4. While the unconstrained pseudo-Voigt fitting consistently achieved the highest R^2 values, it also generated the largest linewidth estimations due to the excessive Lorentzian contribution. Conversely, the baseline-corrected Gaussian

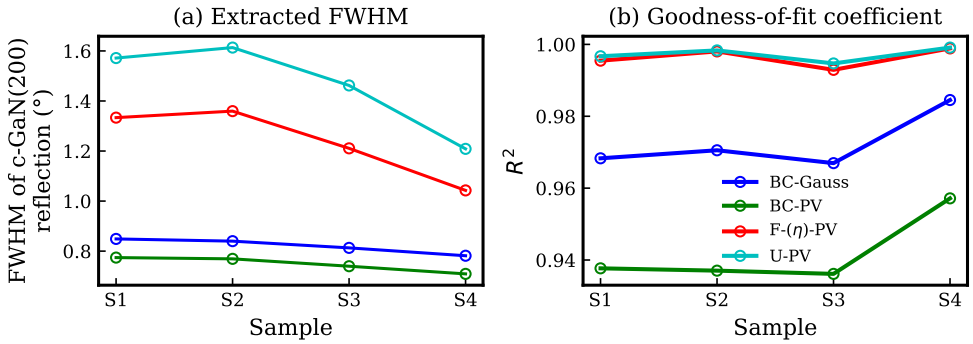


Fig. 4: Comparison of the extracted FWHM values and goodness-of-fit coefficients (R^2) obtained from the different peak-profile fitting methodologies. Although the unconstrained pseudo-Voigt fitting yields the highest R^2 values, it simultaneously produces the largest linewidth estimations due to excessive Lorentzian broadening.

fitting produced slightly lower R^2 values but significantly improved consistency in the evolution of FWHM, crystallite size, and defect density. The systematic reduction in linewidth obtained using the Gaussian-baseline methodology suggests a progressive improvement in crystalline quality from S1 to S4. This behavior is consistent with reduced defect-related broadening, increased crystalline coherence, and the beneficial effect of the low-temperature GaN buffer layer on the structural quality of cubic GaN films.

A substantial reduction in linewidth was obtained after implementing local baseline subtraction. Both the baseline-corrected pseudo-Voigt and Gaussian fitting approaches produced a systematic decrease in FWHM from S1 to S4, indicating a progressive improvement in crystalline coherence. These results demonstrate that appropriate background treatment plays a critical role in obtaining physically meaningful linewidth estimations from X-ray diffraction data.

The Gaussian fitting methodology exhibited the most stable linewidth evolution among the analyzed strategies, providing a physically consistent trend that closely follows the expected improvement in crystal quality associated with the introduction of the low-temperature GaN buffer layer [26]. Table 1 summarizes the peak-position, linewidth, profile-shape, and goodness-of-fit parameters extracted from the different fitting methodologies.

The structural implications of the extracted linewidth evolution are summarized in Figure 5 and Figure 6. Using the baseline-corrected Gaussian fitting results, the normalized evolution of FWHM, crystallite size, and threading dislocation density reveals a clear correlation between linewidth narrowing and structural improvement. As the FWHM decreases from sample S1 to S4, the estimated crystallite size increases while the calculated threading dislocation density decreases [27].

Table 1: Comparison of FWHM and goodness-of-fit values obtained from the different fitting strategies for the c-GaN(200) reflection.

Fitting strategy	Sample	2θ (deg)	FWHM (deg)	η	R^2
Unconstrained PV	S1	40.162	1.572	1.0	0.9967
Unconstrained PV	S2	40.082	1.613	1.0	0.9983
Unconstrained PV	S3	40.102	1.462	1.0	0.9947
Unconstrained PV	S4	40.110	1.209	1.0	0.9991
Fixed-η PV	S1	40.165	1.333	0.5	0.9955
Fixed-η PV	S2	40.091	1.359	0.5	0.9980
Fixed-η PV	S3	40.103	1.211	0.5	0.9929
Fixed-η PV	S4	40.111	1.043	0.5	0.9989
Baseline-corrected PV	S1	40.111	0.774	0.3	0.9377
Baseline-corrected PV	S2	40.064	0.769	0.3	0.9370
Baseline-corrected PV	S3	40.081	0.740	0.3	0.9361
Baseline-corrected PV	S4	40.091	0.709	0.3	0.9572
Baseline-corrected Gaussian	S1	40.110	0.849	–	0.9683
Baseline-corrected Gaussian	S2	40.066	0.840	–	0.9705
Baseline-corrected Gaussian	S3	40.077	0.813	–	0.9670
Baseline-corrected Gaussian	S4	40.089	0.782	–	0.9845

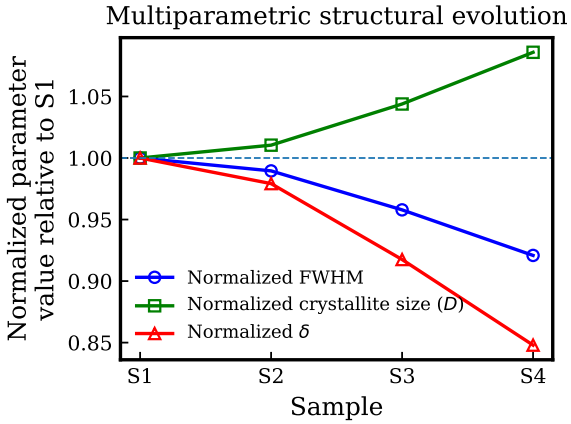


Fig. 5: Normalized evolution of FWHM, crystallite size, and threading dislocation density obtained from the baseline-corrected Gaussian fitting methodology. The figure highlights the correlation between linewidth reduction, enhanced crystalline coherence, and defect-density suppression from samples S1 to S4.

Table 2: Structural parameters extracted from the baseline-corrected Gaussian fitting of the c-GaN(200) reflection.

Sample	2θ (deg)	FWHM (deg)	D (nm)	$\delta_{\mathrm{Scherrer}}$ (cm^{-2})	$\delta_{\mathrm{Frentrup}}$ (cm^{-2})
S1	40.110	0.849	9.96	1.01×10^{12}	4.96×10^{10}
S2	40.066	0.840	10.07	9.87×10^{11}	4.86×10^{10}
S3	40.077	0.813	10.40	9.24×10^{11}	4.55×10^{10}
S4	40.089	0.782	10.82	8.54×10^{11}	4.21×10^{10}

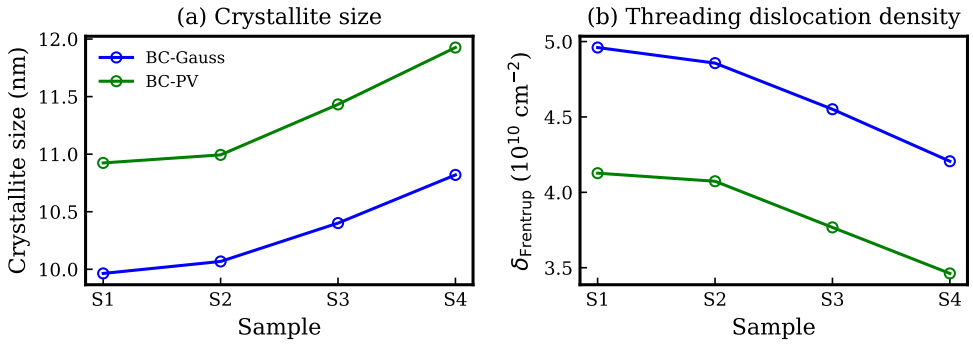


Fig. 6: Evolution of (a) crystallite size (13) and (b) threading dislocation density (15) calculated from the baseline-corrected pseudo-Voigt and Gaussian fitting approaches. Both methodologies reveal progressive structural improvement across the sample series. However, a BC-PV fitting strategy could lead to an overestimation of the crystallite size and, hence, a lower estimated threading dislocation density.

The apparent crystallite size (D) values were extracted by using the Scherrer equation (13) and the threading dislocation density δ_{Scherrer} and δ_{Frentrup} were estimated from the Scherrer relation (14) and the random-distribution mosaic model (15) reported in [28], respectively.

$$D = \frac{K\lambda}{\beta \cos\theta} \tag{13}$$

where:

- $K = 0.9$ is the Scherrer constant,
- $\lambda = 0.15406$ nm is the Cu Kα wavelength,
- β is the FWHM in radians,
- θ is the Bragg angle.

$$\delta_{Scherrer} = \frac{1}{D^2} \tag{14}$$

$$\delta_{Frentrup} = \frac{\beta^2}{4.35b^2}, \tag{15}$$

where $b = a_{zb}/\sqrt{2}$ is the Burgers vector of zincblende GaN and β is the fitted linewidth expressed in radians. Although this model is commonly applied to tilt/twist broadening extracted from rocking-curve measurements, it is employed here as a comparative estimate based on the c-GaN(200) linewidth evolution. Therefore, δ_{Frentrup} should be interpreted only as a comparative indicator rather than an absolute threading dislocation density.

The quantitative values extracted are summarized in Table 2. The crystallite size increased systematically across the sample series, whereas the estimated threading dislocation density exhibited a corresponding reduction. This behavior suggests a progressive enhancement of crystalline coherence [29] and a reduction in defect-related

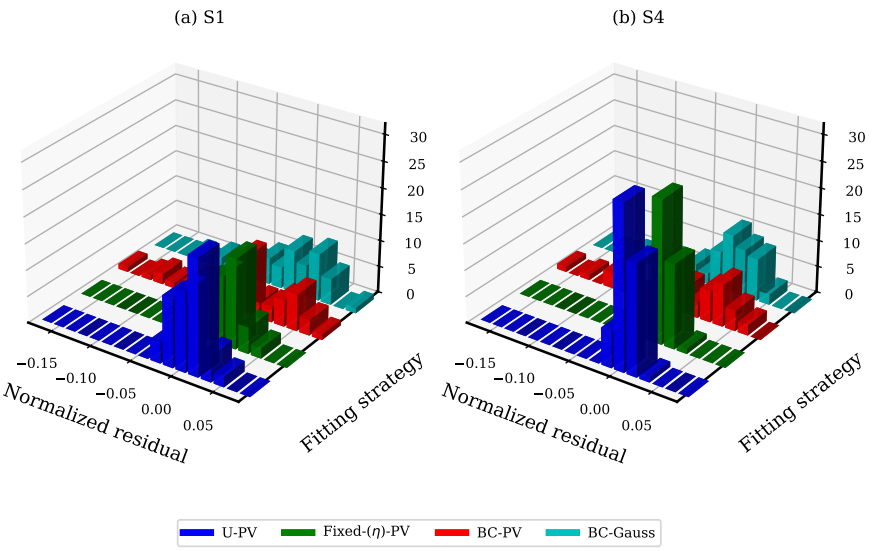


Fig. 7: Residual analysis of the different peak-profile fitting methodologies. Panels (a) and (b) show the normalized residual profiles for samples S1 and S4, respectively, through the corresponding three-dimensional residual histograms, illustrating the statistical distribution of fitting errors for each fitting strategy.

broadening mechanisms [19], supporting the effectiveness of the low-temperature buffer layer in improving the structural quality of the c-GaN epilayers [30]. The crystallite sizes derived from the Scherrer equation should be interpreted as coherence lengths, since residual contributions from strain and instrumental broadening may still be present.

Because the present study focuses on the comparative evolution of the c-GaN(200) linewidth among samples measured under identical experimental conditions, the extracted crystallite sizes should be regarded as relative indicators of crystalline coherence. Therefore, the observed trends are more significant than the absolute values obtained from the Scherrer equation.

Additional insight into the fitting performance is provided by the residual analysis shown in Figure 7. The residual profiles and three-dimensional residual histograms reveal that the unconstrained pseudo-Voigt fitting produced the narrowest residual distributions and the highest coefficients of determination (R^2). Nevertheless, this apparent numerical superiority did not translate into physically meaningful linewidth evolution. In contrast, the baseline-corrected fitting approaches yielded slightly broader residual distributions while simultaneously producing more realistic linewidth values and more consistent structural parameter trends.

This observation highlights an important aspect of XRD peak-profile analysis: the fitting methodology that minimizes statistical error does not necessarily provide the most physically representative description of the diffraction broadening mechanisms

[31]. Consequently, the selection of an appropriate profile shape and baseline treatment becomes essential for reliable comparative structural analysis of c-GaN thin films [28].

These results demonstrate that maximizing the numerical goodness-of-fit alone is insufficient for reliable structural characterization. Instead, physically meaningful linewidth evolution should be considered together with conventional fitting metrics when evaluating peak-profile fitting methodologies.

Overall, the comparative analysis demonstrates that baseline treatment exerts a greater influence on linewidth reliability than the specific analytical form of the peak profile. The baseline-corrected Gaussian fitting approach provided the most physically consistent description of the c-GaN(200) diffraction peak, yielding a monotonic linewidth reduction, realistic crystallite-size evolution, and defect-density trends that agree with the expected structural improvement induced by buffer-assisted growth optimization. Therefore, this methodology was selected as the most suitable approach for comparative linewidth analysis of the investigated c-GaN thin films.

4 Conclusions

The detailed recalibration analysis of the c-GaN(200) diffraction peak demonstrates that the extracted linewidth parameters are highly sensitive to the selected fitting strategy, baseline treatment, and peak-profile assumptions. Although all evaluated fitting approaches reproduced the experimental diffraction data with comparable statistical quality, significant variations were observed in the resulting FWHM values and, consequently, in the derived microstructural parameters. In particular, unconstrained pseudo-Voigt fitting systematically converged toward an almost purely Lorentzian profile, revealing a pronounced sensitivity to asymmetric peak tails and residual background contributions. The implementation of profile-shape constraints together with local baseline correction progressively mitigated these effects and produced more physically meaningful linewidth estimations.

Among the evaluated approaches, nonlinear Gaussian fitting combined with local baseline subtraction provided the most stable and physically consistent evolution of the c-GaN(200) linewidths across the sample series. This methodology revealed a systematic decrease in FWHM from S1 to S4, accompanied by an increase in the apparent crystallite size and a corresponding reduction in the estimated threading dislocation density. Although the absolute values of these parameters depend on the adopted broadening model, the relative trends remained consistent across all recalibration strategies.

The convergence of independent fitting methodologies toward the same overall trend provides strong evidence that the structural improvement observed for sample S4 is intrinsic and not an artifact of the fitting procedure. Moreover, the excellent agreement between XRD linewidth analysis and AFM characterization further supports the conclusion that the incorporation of a low-temperature GaN buffer layer promotes enhanced crystalline quality, improved cubic-phase stabilization, and reduced defect-related broadening mechanisms.

Beyond the specific case of cubic GaN heteroepitaxy, this study highlights the limitations of relying exclusively on conventional goodness-of-fit metrics for diffraction

peak analysis. Reliable structural characterization requires the simultaneous consideration of physically meaningful linewidth evolution, appropriate background treatment, and consistency with complementary characterization techniques. The methodology established here provides a robust framework for comparative XRD linewidth analysis of semiconductor thin films and offers additional evidence of the structural benefits associated with buffer-assisted growth optimization.

Acknowledgments

The authors acknowledge D. Ramirez for technical assistance during the synthesis of the structures, A. Tavira for support with X-ray diffraction measurements, and M. Avendaño for AFM measurements.

Funding:

This work was supported by SECIHTI and CINVESTAV through institutional research facilities and infrastructure support.

CRediT

Y. Hernández Barrios: Conceptualization, methodology, Formal analysis, Writing - Original Draft, Writing - Review and Editing. **J.A.Santis:** Validation, Formal analysis, Resources, Supervision, Project administration, review and editing. **B. Moreno-Juan:** Data Curation, review and editing, Visualization. **J.G. Sánchez López:** Data Curation, review and editing, Visualization. **S. Garduño Vértiz:** Data Curation, Supervision, review and editing,Visualization. **J.Juan Diaz:** Data curation, review and editing, Visualization.

All authors reviewed and approved the final version of the manuscript.

data

The data that support the findings of this study are available from the corresponding author upon reasonable request.

supplementary data

No supplementary data are available for this article.

Declarations

This article does not contain any studies with human participants or animals performed by any of the authors. Therefore, ethical approval and consent are not applicable. Ethics, consent to participate, and consent to publish declarations Not applicable.

Competing interests

The authors declare no competing interests.

References

[1] Ungár, T.: Microstructural parameters from x-ray diffraction peak broadening. Scripta Materialia **51**(8), 777–781 (2004) https://doi.org/10.1016/j.scriptamat.2004.05.007 . Viewpoint set no. 35. Metals and alloys with a structural scale from the micrometer to the atomic dimensions

[2] Ortiz-Cruz, A., Santolalla, C., Moreno, E., Reyes-Heredia, J.A., Alvarez-Ramirez, J.: Fractal analysis of powder x-ray diffraction patterns. Physica A: Statistical Mechanics and its Applications **391**(4), 1642–1651 (2012) https://doi.org/10.1016/j.physa.2011.10.008

[3] Krost, A., Dadgar, A., Schulze, F., Clos, R., Haberland, K., Zettler, T.: Heteroepitaxy of gan on silicon: In situ measurements. In: Silicon Carbide and Related Materials 2004. Materials Science Forum, vol. 483, pp. 1051–1056. Trans Tech Publications Ltd, ??? (2005). https://doi.org/10.4028/www.scientific.net/MSF.483-485.1051

[4] Kemper, R.M., Häberlen, M., Schupp, T., Weinl, M., Bürger, M., Ruth, M., Meier, C., Niendorf, T., Maier, H.J., Lischka, K., As, D.J., Lindner, J.K.N.: Formation of defects in cubic gan grown on nano-patterned 3c-sic (001). physica status solidi c **9**(3–4), 1028–1031 (2012) https://doi.org/10.1002/pssc.201100174 https://onlinelibrary.wiley.com/doi/pdf/10.1002/pssc.201100174

[5] Scardi, P.: Diffraction line profiles in the rietveld method. Crystal Growth & Design **20**(10), 6903–6916 (2020) https://doi.org/10.1021/acs.cgd.0c00956 https://doi.org/10.1021/acs.cgd.0c00956

[6] Coelho, A.A.: *TOPAS* and *topas-academic*: an optimization program integrating computer algebra and crystallographic objects written in c++. Journal of Applied Crystallography **51**(1), 210–218 (2018) https://doi.org/10.1107/S1600576718000183

[7] Scardi, P., D'Incau, M., Malagutti, M.A., Terban, M.W., Hinrichsen, B., Fitch, A.N.: A reference material for x-ray diffraction line profile analysis. Journal of Applied Crystallography **58**(5), 1764–1777 (2025) https://doi.org/10.1107/S1600576725006946

[8] Harrington, G.F., Santiso, J.: Back-to-basics tutorial: X-ray diffraction of thin films. Journal of Electroceramics **47**(4), 141–163 (2021) https://doi.org/10.1007/s10832-021-00263-6

[9] Dinnebier, R., Scardi, P.: X-ray powder diffraction in education. part i. bragg

peak profiles. Journal of Applied Crystallography **54**(6), 1811–1831 (2021) https://doi.org/10.1107/S1600576721009183

[10] Monshi, A., Foroughi, M.R., Monshi, M.R.: Modified scherrer equation to estimate more accurately nano-crystallite size using xrd. World Journal of Nano Science and Engineering **2**(3), 154–160 (2012) https://doi.org/10.4236/wjnse.2012.23020

[11] Nath, D., Singh, F., Das, R.: X-ray diffraction analysis by williamson-hall, halder-wagner and size-strain plot methods of cdse nanoparticles: a comparative study. Materials Chemistry and Physics **239**, 122021 (2020) https://doi.org/10.1016/j.matchemphys.2019.122021

[12] Hargreaves, J.S.J.: Some considerations related to the use of the scherrer equation in powder x-ray diffraction as applied to heterogeneous catalysts. Catalysis, Structure & Reactivity **2**(1–4), 33–37 (2016) https://doi.org/10.1080/2055074X.2016.1252548

[13] Santis, J.A., Marín-García, C.A., Sánchez-R., V.M.: Effect of different substrates on material properties of cubic gan thin films grown by lp-mocvd method. Journal of Crystal Growth **601**, 126944 (2023) https://doi.org/10.1016/j.jcrysgro.2022.126944

[14] Lee, J., Bayram, C.: In: Kizilyalli, I.C., Han, J., Speck, J.S., Carlson, E.P. (eds.) Cubic GaN: Growth, Characterization, and Applications, pp. 617–639. Springer, Cham (2025). https://doi.org/10.1007/978-3-031-83056-3_26 . https://doi.org/10.1007/978-3-031-83056-3_26

[15] Binks, D.J., Dawson, P., Oliver, R.A., Wallis, D.J.: Cubic gan and ingan/gan quantum wells. Applied Physics Reviews **9**(4), 041309 (2022) https://doi.org/10.1063/5.0097558

[16] Freitas, J. Jaime A., Culbertson, J.C., Storm, D.F., Mahadik, N.A., Nepal, N., Anderson, T.J.: Structural and optical properties of cubic gan films on high-thermal conductivity substrates. Journal of Applied Physics **137**(3), 035101 (2025) https://doi.org/10.1063/5.0204660

[17] Gu, S., Zhang, R., Shi, Y., Zheng, Y., Zhang, L., Dwikusuma, F., Kuech, T.F.: The impact of initial growth and substrate nitridation on thick gan growth on sapphire by hydride vapor phase epitaxy. Journal of Crystal Growth **231**(3), 342–351 (2001) https://doi.org/10.1016/S0022-0248(01)01464-6 . Proceedings of the International Specialist Meeting on Bulk Nitrides and Related Techniques

[18] Marín-García, C.A., Arias-Cerón, J.S., Sánchez-R., V.M.: Longitudinal optical raman mode a1 to calculate the indium molar fraction of epitaxial ingan layers grown by lp-mocvd on polar and non-polar planes. Journal of Materials Science: Materials in Electronics **31**(10), 7455–7460 (2020) https://doi.org/10.1007/

s10854-020-02966-y

[19] Moram, M.A., Johnston, C.F., Kappers, M.J., Humphreys, C.J.: The effects of film surface roughness on x-ray diffraction of nonpolar gallium nitride films. Journal of Physics D: Applied Physics **42**(13), 135407 (2009) https://doi.org/10.1088/0022-3727/42/13/135407

[20] Pan, Z., Chen, Z., Chen, Y., Zhang, H., Yang, H., Hu, L., Kang, X., Yuan, Y., Jia, C., Liang, Z., Wang, Q., Zhang, G., Shen, B.: Effect of grain coalescence on dislocation and stress in gan films grown on nanoscale patterned sapphire substrates. CrystEngComm **26**(5), 620–630 (2024) https://doi.org/10.1039/D3CE00987D

[21] Bazioti, C., Papadomanolaki, E., Kehagias, T., Walther, T., Smalc-Koziorowska, J., Pavlidou, E., Komninou, P., Karakostas, T., Iliopoulos, E., Dimitrakopulos, G.P.: Defects, strain relaxation, and compositional grading in high indium content ingan epilayers grown by molecular beam epitaxy. Journal of Applied Physics **118**(15), 155301 (2015) https://doi.org/10.1063/1.4933276

[22] Ungár, T., Gubicza, J., Ribárik, G., Borbély, A.: Crystallite size distribution and dislocation structure determined by diffraction profile analysis: principles and practical application to cubic and hexagonal crystals. Journal of Applied Crystallography **34**(3), 298–310 (2001) https://doi.org/10.1107/S0021889801003715

[23] Scardi, P., Leoni, M.: Line profile analysis: pattern modelling *versus* profile fitting. Journal of Applied Crystallography **39**(1), 24–31 (2006) https://doi.org/10.1107/S0021889805032978

[24] Ida, T., Ando, M., Toraya, H.: Extended pseudo-voigt function for approximating the voigt profile. Journal of Applied Crystallography **33**(6), 1311–1316 (2000) https://doi.org/10.1107/S0021889800010219

[25] Himabindu, B., Latha Devi, N.S.M.P., Rajini Kanth, B.: Microstructural parameters from x-ray peak profile analysis by williamson-hall models: a review. Materials Today: Proceedings **47**, 4891–4896 (2021) https://doi.org/10.1016/j.matpr.2021.06.256 . FRESM'21

[26] Zhao, J., Suo, B., Xu, R., Tao, T., Zhuang, Z., Liu, B., Zhang, X., Chang, J.: Effects of buffer layer on structural properties of nonpolar $(11\bar{2}0)$-plane gan film. Crystals **13**(7) (2023) https://doi.org/10.3390/cryst13071145

[27] Shen, X.Q., Matsuhata, H., Okumura, H.: Reduction of the threading dislocation density in gan films grown on vicinal sapphire (0001) substrates. Applied Physics Letters **86**(2), 021912 (2005) https://doi.org/10.1063/1.1849836

[28] Frentrup, M., Lee, L.Y., Sahonta, S.-L., Kappers, M.J., Massabuau, F., Gupta, P., Oliver, R.A., Humphreys, C.J., Wallis, D.J.: X-ray diffraction analysis of cubic zincblende iii-nitrides. Journal of Physics D: Applied Physics **50**(43), 433002

(2017) https://doi.org/10.1088/1361-6463/aa865e

[29] Tellekamp, M.B., Miller, M.K., Zhou, L., Tamboli, A.: Structure, defects, and optical properties of commensurate gan/zngen$_2$/gan double heterojunctions. J. Mater. Chem. C **11**(40), 13917–13923 (2023) https://doi.org/10.1039/D3TC02425C

[30] Hoshino, K., Yanagita, N., Araki, M., Tadatomo, K.: Effect of low-temperature gan buffer layer on the crystalline quality of subsequent gan layers grown by movpe. Journal of Crystal Growth **298**, 232–234 (2007) https://doi.org/10.1016/j.jcrysgro.2006.10.189 . Thirteenth International Conference on Metal Organic Vapor Phase Epitaxy (ICMOVPE XIII)

[31] Benedetti, A., Fagherazzi, G., Enzo, S., Battagliarin, M.: A profile-fitting procedure for analysis of broadened x-ray diffraction peaks. ii. application and discussion of the methodology. Journal of Applied Crystallography **21**(5), 543–549 (1988) https://doi.org/10.1107/S0021889888006624